28 May 2010, 2:00 pm - 3:30 pm

Dynamic Response of Cantilever Retaining Walls Considering Soil Non-Linearity

Leuzzi Francesco
Politecnico di Torino, Italy

S. Foti
Politecnico di Torino, Italy

R. Lancellotta
Politecnico di Torino, Italy

G. Mylonakis
University of Patras, Greece

Fifth International Conference on
Recent Advances in Geotechnical Earthquake Engineering and Soil Dynamics
and Symposium in Honor of Professor I.M. Idriss
May 24-29, 2010 • San Diego, California

DYNAMIC RESPONSE OF CANTILEVER RETAINING WALLS CONSIDERING SOIL NON-LINEARITY

Leuzzi Francesco
Politecnico di Torino, 24 Corso Duca degli Abruzzi
10129 Torino, ITALY

Foti S.[*], Lancellotta R.[*], Mylonakis G.[**]
[*] Politecnico di Torino, 24 Corso Duca degli Abruzzi
10129 Torino, ITALY
[**] University of Patras, 26500 Rion (Patras), GREECE

ABSTRACT

For many decades the analysis of earth retaining structures under dynamic or seismic conditions has been carried out by means of standard limit equilibrium (Coulomb, M-O) or elastic methods (Wood, Veletsos and Younan).
These approaches are simplified, as they make use of considerable approximations which are often applicable only under particular conditions. A different and perhaps more realistic approach is possible using established computer codes, which integrate numerically the governing equations of the soil and wall media. Since these problems may involve significant levels of strain in the backfill, material non-linearity should be taken into account to realistically simulate the response of the system. In the herein-reported study, a parametric analysis is carried out through the finite-difference code FLAC 5.0.
Starting from simple cases involving elastic response, and moving gradually towards more realistic conditions, salient features of the dynamic wall-soil interaction problem are addressed. The case of non-linear hysteretic behaviour of soil and flexibility of wall is considered at a second stage. Results indicate that with increasing levels of acceleration, there is a clear transition from elastic behaviour (in which the aforementioned V-Y type methods are applicable), to plastic behaviour in which M-O methods are thought to be more suitable under pseudo-static conditions. The results of the parametric analyses are reported in terms of pertinent normalized parameters, to provide a general framework for the assessment of wall-soil dynamic interaction under strong seismic excitation.

INTRODUCTION

Analysis and design of earth retaining structures under seismic conditions poses a challenging problem, as the mechanics of wall-soil interaction are not well understood. Dynamic soil-structure interaction effects are dominant and should be taken into account in the assessment and quantification of the problem.
Analysis procedures can be roughly classified into two main groups: pseudo-static limit equilibrium approaches based on the well-known Mononobe and Okabe solution (Mononobe and Matsuo [1929], Okabe [1926]) and its variants, and elastic approaches following the seminal works by Wood [1973], Arias *et al.* [1981] and, more recently, Veletsos and Younan [1994, 1997].
The first group of methods is essentially an extension of Coulomb's classical solution, including additional inertial forces due to seismic shaking. The method has been extensively studied and modified (Seed and Whitman [1970], Richards and Elms [1979]), and it is widely used for the analysis and design of both rigid and flexible structures, regardless of the actual amount of wall displacement associated with the formation of a failure surface.
Ways to account for wall flexibility have been developed in the realm of the second group of methods, leading to certain closed-form solutions for visco-elastic soil (Wood [1973], Arias *et al.* [1981]). These solutions are often considered unduly conservative, as the kinematical constraint associated with a rigid wall generates pressures twice as large as those predicted by the M-O formula. Recent work by Veletsos and Younan [1994, 1997] has shown a significant reduction of pressures with increasing wall flexibility and/or base compliance.
Notwithstanding the theoretical significance and practical appeal of the above methods, they can both be criticized for making use of considerable approximations, which are applicable only under particular conditions. A different and perhaps more realistic approach is possible using established numerical methods, which aim at integrating in space and time the governing differential equations of the soil and wall media. Since these problems may involve significant levels of strain in the backfill, material non-linearity should be taken into account to realistically simulate the response of the system. In the

herein-reported study, a parametric analysis is carried out by means of the finite-difference code FLAC.
Starting from simple elastic analyses and progressing to more realistic cases, salient features of dynamic wall-soil interaction problem are addressed. Two basic systems have been analyzed under both pseudo-static and dynamic conditions: a homogenous elastic backfill retained by a vertical cantilever wall, and a vertically inhomogeneous backfill, characterized by a parabolic or exponential variation of soil stiffness with depth. In the first case, walls varying from rigid to flexible, with or without rotational base compliance, are simulated. In the second case, the effect of soil inhomogeneity is investigated for a wide class of walls and soil configurations.
Moving towards more realistic conditions, the case of flexible vertical cantilever wall retaining a horizontal layer of inhomogeneous backfill, obeying an elastic-plastic Mohr-Coulomb criterion, is analyzed. The excitation consists of a single-cycle sinusoidal pulse with a given amplitude and frequency applied at the bottom of the model.
The results of the parametric analyses are reported in terms of pertinent normalized parameters, to provide a general framework for the assessment of soil-wall dynamic interaction under strong seismic excitation.

ELASTIC PROBLEM

In this section, the models used for the simulation of the elastic problem for both homogeneous and inhomogeneous soil, and corresponding results are reported. Results have been compared, whenever possible, with available closed-form solutions.

Homogeneous Case

The system consists of a semi-infinite layer of visco-elastic material of height H retained along one of its vertical boundaries by a uniform flexible cantilever retaining wall restrained by a rotational spring of stiffness R_θ at its base. The system is excited by a harmonic horizontal motion, as shown in fig. 1.
The properties of the soil are:

- Mass density: ρ
- Shear modulus: G
- Poisson's ratio: ν
- Material damping factor: β

The properties of the wall are:

- Thickness: t_w
- Mass per unit surface area: μ_w
- Young's modulus: E_w
- Poisson's ratio ν_w
- Material damping factor: β_w

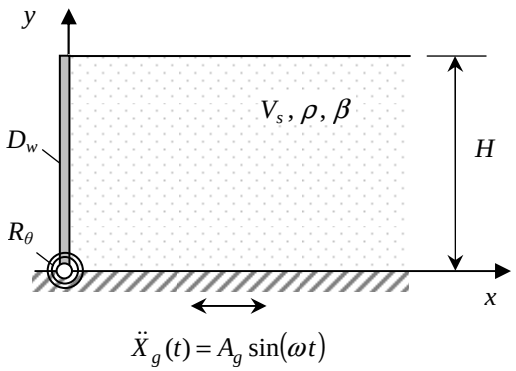

Fig. 1. Elastic model

The relevant parameters for a parametric analysis are the relative flexibility between wall and retained soil d_w, defined by:

$$d_w = \frac{GH^3}{D_w} \tag{1}$$

where D_w is the flexural rigidity of the wall:

$$D_w = \frac{E_w t_w^3}{12(1-\nu_w^2)} \tag{2}$$

and the relative flexibility between rotational base constraint and retained soil d_θ, defined by:

$$d_\theta = \frac{GH^2}{R_\theta} \tag{3}$$

The elastic soil is characterized by uniform shear wave velocity V_s = 100 m/s and mass density ρ = 1.8 Mg/m^3, therefore G = 18 MPa. Furthermore, Poisson's ratio is assumed to be ν = 1/3 and the material damping factor β = 5%. The grid dimensions are (0.5 x 0.5 m).
The height of the wall is H = 8 m and it is discretized by means of beam elements of unit longitudinal dimension and thickness t_w = 0.20 m. The mass per unit of surface area is assumed μ_w = 2.5 Mg/m^2. It's worthwhile to mention that V-Y solution was obtained based on the assumption of a massless wall. The Young's modulus of the wall can be linked to the other parameters using equations (1) and (2) (as already done by Psarropoulos *et al.* [2005]):

$$E_w = \frac{12GH^3\left(1-\nu_w^2\right)}{d_w t_w^3} \tag{4}$$

The values of d_w assumed here are 0 (for rigid wall), 1, 5 and 40; the values of d_θ are 0 (for a fixed base wall), 0.5, 1 and 5.
The interface between the soil and the wall was selected as bonded in order to permit a comparative study against available closed-form solutions (see fig. 2).

When the frequency of excitation, ω, is very low compared to the fundamental frequency of the soil layer, ω_1, the excitation will be referred to as '*static*', a term which should not be confused with that normally used to represent the effects of gravity forces. To avoid possible confusion, in the ensuing the term *pseudo-static* loading will be used. In this case it's more convenient to replace the excitation with a set of horizontal body forces equal to $\rho \cdot \left(\ddot{X}_g(t)\right)_{\max} = \rho \cdot A_g$ applied to all grid nodes, as shown in fig. 2.

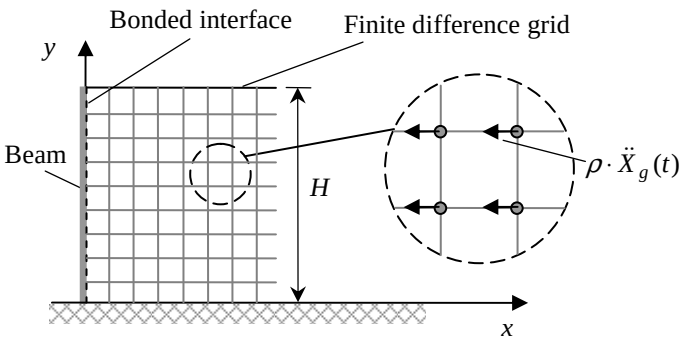

Fig. 2. Pseudo-Static seismic loading via equivalent body forces in wall and soil

To achieve convergence of the model, the pseudo-static load was applied gradually in several steps.
The results are normalized according to the following factors:

- Horizontal pressures:

$$\frac{\sigma_{st}}{\alpha_g \gamma H} \tag{5}$$

where $\alpha_g = A_g / g$ is the maximum horizontal ground acceleration expressed in g, $\gamma = \rho g$ is the unit weight of the soil;

- Base shear:

$$\frac{V_b}{\alpha_g \gamma H^2} \tag{6}$$

- Base moment:

$$\frac{M_b}{\alpha_g \gamma H^3} \tag{7}$$

- Effective height:

$$\frac{h}{H} = \frac{M_b}{H V_b} \tag{8}$$

which defines the point of application of the resultant force, measured from the base of the wall;

- Wall displacements:

$$\frac{w G}{\alpha_g \gamma H^2} \tag{9}$$

Notice that the results reported in the ensuing encompass exclusively horizontal shaking, *i.e.* to determine the complete state of stress, the initial stresses due to gravity loads should be added.
Figure 3 shows the heightwise distribution of the horizontal pressures on the wall, determined by V-Y, as function of relative wall flexibility (fig. 3a), and relative base flexibility (fig. 3b) ($\eta = y / H$ is the normalized height). Results of analyses with FLAC have been compared with same simulations with the FEM code PLAXIS. Figures 4 and 5 show, respectively, the case of fixed base wall and rigid wall; PLAXIS results are displayed with solid line, whereas FLAC results are depicted with dots.
The numerical results are in a very good agreement with the results obtained by V-Y, except from the upper part of the wall where some discrepancies are visible. Similar features were also observed by Wood [1973] and Psarropoulos *et al.* [2005], and are probably to the assumption of complete bonding, as well as that of soil homogeneity, which implies finite soil stiffness not to vanish near the top of wall.

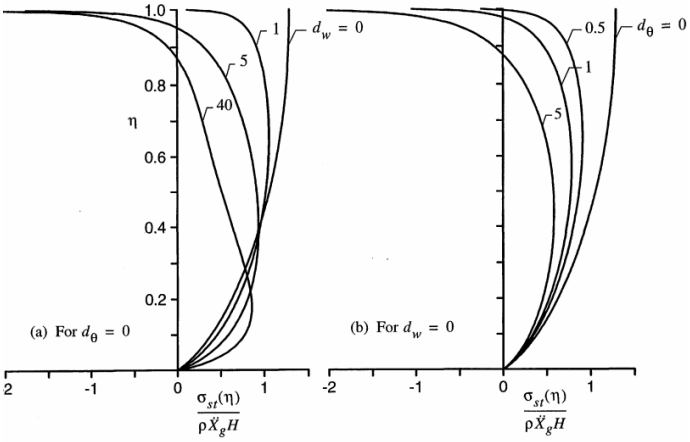

Fig. 3. Wall pressures for different wall and base flexibilities according to Veletsos and Younan [1997]

It's observed that both for large relative wall and base flexibilities, tensile stresses are developing near the top of the wall, clearly stated as a limit of elastic solutions by V-Y, since these tensile stresses can cause de-bonding in case they exceed the value of initial compressive stresses due to gravity.
Figures from 6 to 8 show the variation of normalized base shear (V_b), effective height (h) and top displacements (w) for different d_w and d_θ, whereas solid lines indicate the corresponding closed-form solution results. An excellent agreement is observed, except for the case of rigid walls, where the aforementioned numerical problems play a slightly more important role.

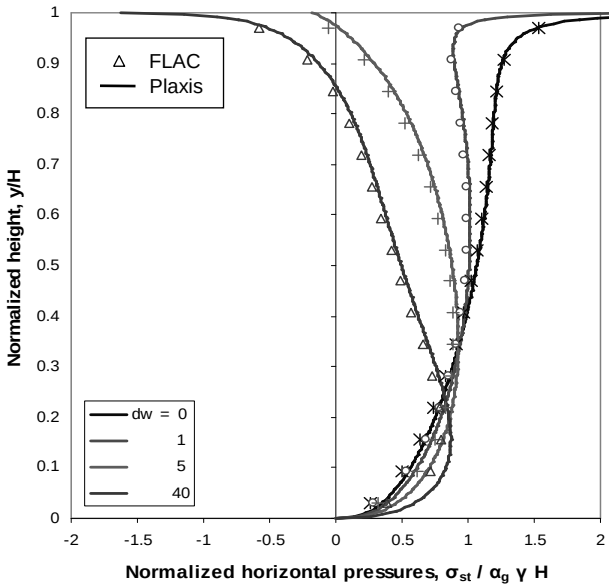

Fig. 4. Wall pressures for a fixed base wall ($d_\theta = 0$)

Note, however, the large reduction in terms of base shear due to both wall and base flexibility, as analytically proved by V-Y, and numerically confirmed by these analyses.
It can be also observed that for the effective height a very good agreement with Seed and Whitman [1970] modification of M-O method (0.6 *H*) is visible for rigid walls, whereas for flexible walls only a reasonable agreement can be found with the Rankine distribution (1/3 *H*), the reason being the large tensile stresses near the top that are "lowering" the effective height.
The comparison for top displacements is once again very good but a little deviation from analytical results is observed, especially for flexible walls or walls with flexible base.
Similar results are found for the dynamic case for which, as analytically shown by Veletsos and Younan [1994, 1997], and numerically by Psarropoulos *et al.* [2005], the dynamic quantities are the product of the corresponding 'static' ones by an appropriate amplification or deamplification factor.

Inhomogeneous Case

The assumption of soil homogeneity, which is practically unrealistic, is one of main limitations of the analyses discussed in the previous section. Indeed, in reality, the soil modulus is likely to increase with depth, that is with confining pressure.
Under this assumption V-Y have analyzed the case of a rigid wall elastically constrained against rotation at the base, from a '*static*' point of view. As proposed by Veletsos and Younan [1994] the inhomogeneity is expressed through a *parabolic* variation of shear modulus with depth (see fig. 9):

$$G(\eta) = G_0\left(1-\eta^2\right) \qquad (10)$$

in which G_0 is the value of shear modulus at the base of the horizontal soil layer.

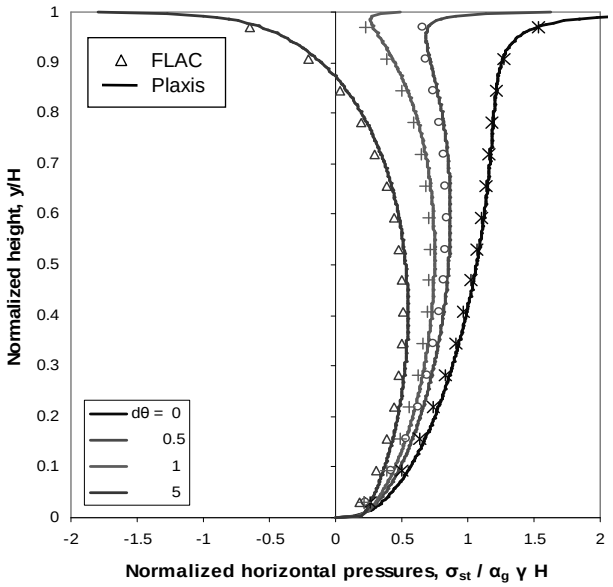

Fig. 5. Wall pressures for a rigid wall ($d_w = 0$)

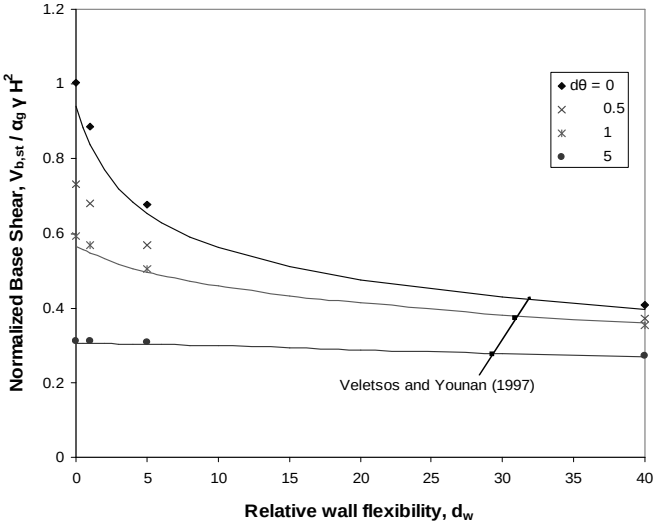

Fig. 6. Normalized base shear for different d_w and d_θ

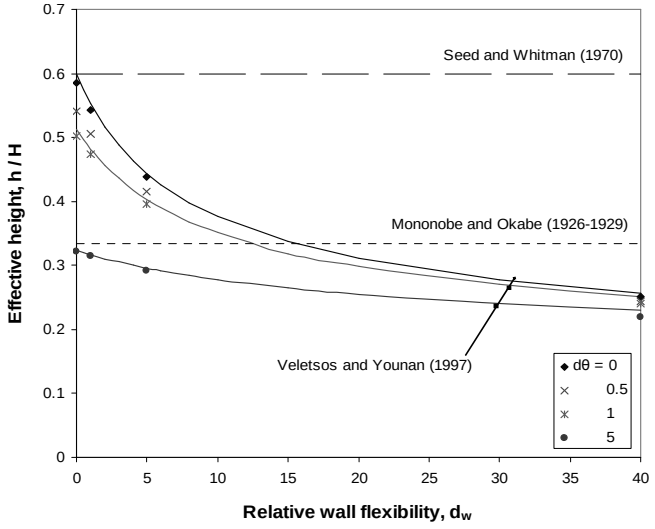

Fig. 7. Normalized effective height for different d_w and d_θ

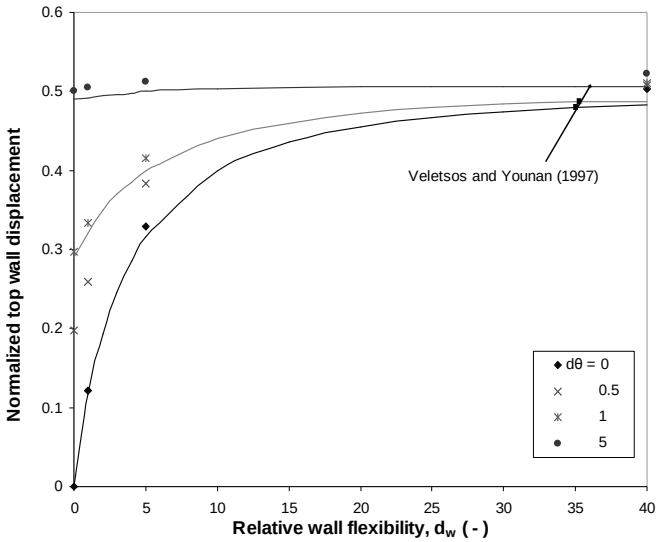

Fig. 8. Wall displacements for different d_w and d_θ

The numerical analyses reported herein are limited to a wall with flexibility (d_w) fixed at the base (d_θ = 0), therefore only the case of rigid wall can be compared with analytical results.
The main parameter of the problem is, again, the relative flexibility of the wall and retained soil, defined by:

$$d_w = \frac{G_{av} H^3}{D_w} \tag{11}$$

where G_{av} is the average value of shear modulus, for this case equal to 2/3 G_0.
The soil stratum considered has an average shear wave velocity $V_{s,av}$ = 100 m/s while the others soil parameters have been maintained to allow a comparative study with the case of homogeneous soil.
The properties of the wall are the same, except its Young's modulus, obtained using relation (4), by substituting G with G_{av}. The values of d_w taken into account are 0 (rigid wall), 1, 5 and 40.
A comparison of pressures for the case of rigid wall is shown in fig. 10: good agreement is observed, except, again for the upper part of the wall, where a value of pressure different from zero is observed, whereas the pressures should be null, as in the solution by V-Y. This is due to the shear modulus near the top, which in the numerical analysis assumes a finite value, as well as the assumption of complete bonding.
In general, the assumption of soil inhomogeineity is responsible for a sensible reduction of stresses.
This is clearly shown in figures 11 and 12, where pressures and bending moments for different wall flexibilities are presented together with corresponding values for the homogeneous case. The reduction is higher for the case of a rigid wall than for a flexible wall, especially in terms of bending moments, and this is due to the fact that for flexible walls both compressive and tensile stresses are lower. The reduction of tensile stresses for flexible walls (d_w = 40) is another important effect arising from the assumption of soil inhomogeneity. Indeed now tensile stresses are practically not influent in the overall behaviour,

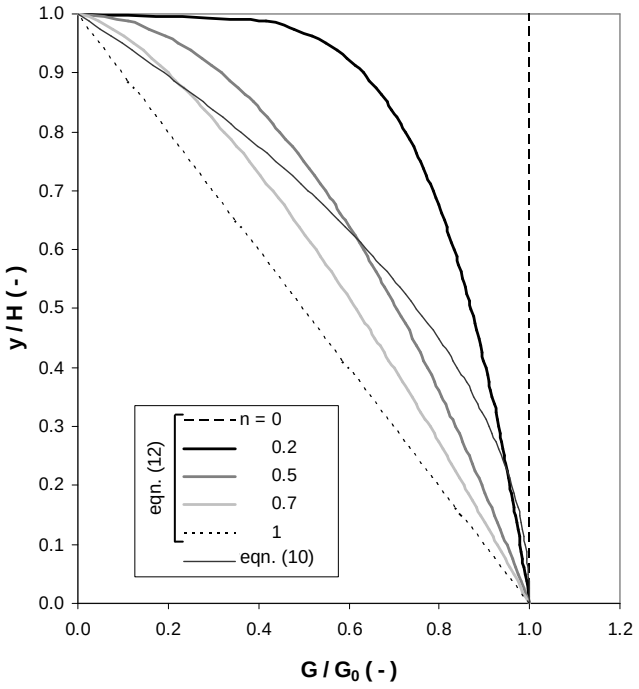

Fig. 9. Different soil inhomogeneities taken into account

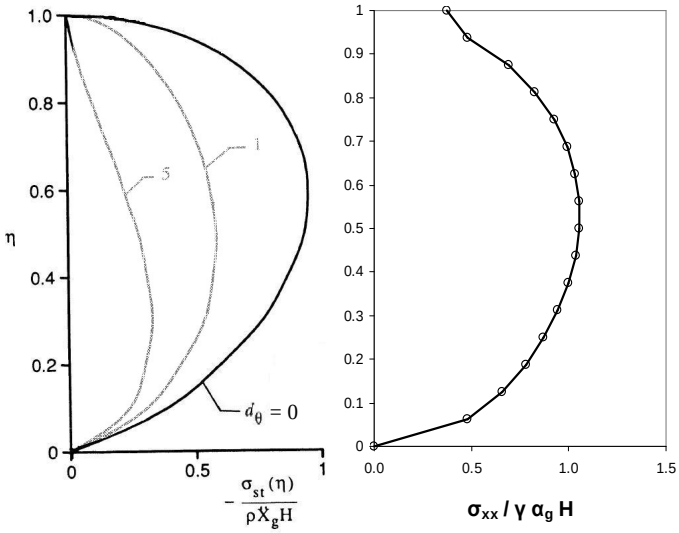

Fig. 10. Parabolic law: comparison of wall pressures for a rigid wall (d_w = 0) (modified from Veletsos and Younan [1994])

and a more realistic simulation of the interaction phenomenon is achieved.
In order to explore in more detail the role of soil inhomogeneity, an *exponential* variation of shear modulus with depth has been taken into account, according to the expression:

$$G(\eta) = G_0 (1-\eta)^n = G_0 \zeta^n \tag{12}$$

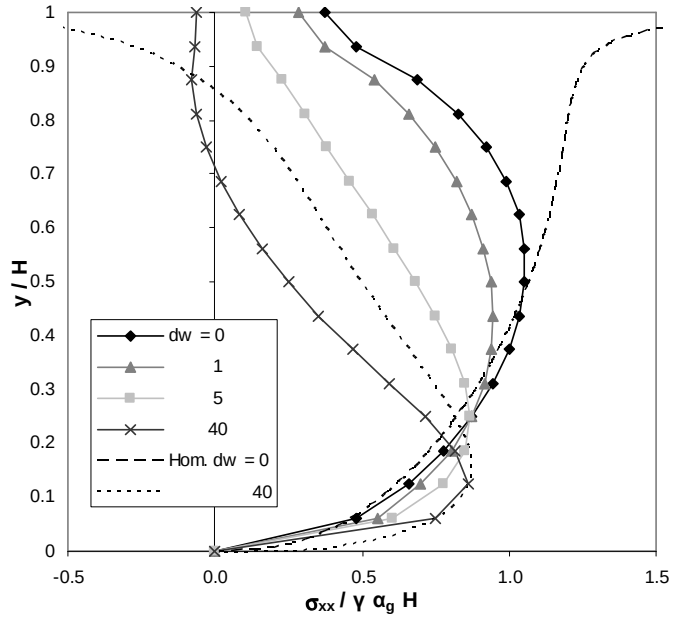

Fig. 11. Parabolic law: wall pressures for different d_w

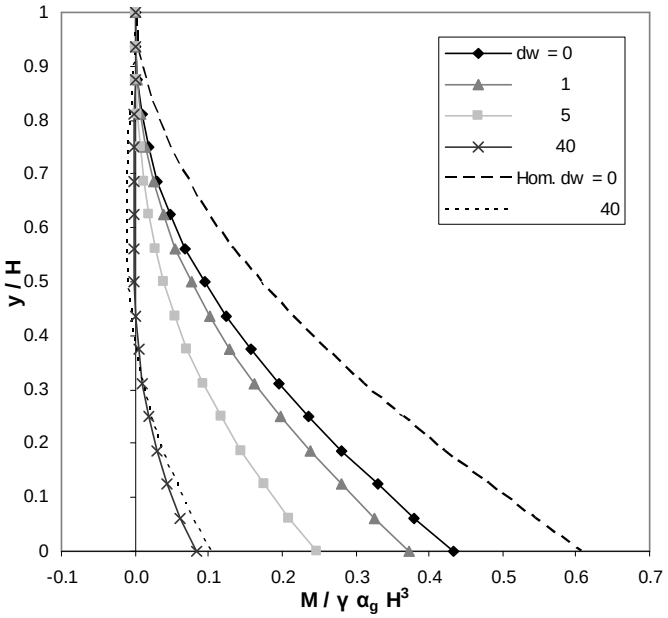

Fig. 12. Parabolic law: bending moments for different d_w

in which:

- G_0 is again the shear modulus at the base of the layer
- $\zeta = z / H = 1 - \eta$ is the normalized depth
- n is a soil inhomogeneity exponent (fig. 9):
  - $n = 0$ represents the case of homogenous soil
  - $n = 1$ the case of linear variation with depth.

The exponent n has been assumed equal to 0.2, 0.5, 0.7 (fig. 9): particularly important is the case $n = 0.5$ which reproduces the observed increase of G in loose coarse grained soils.

Figure 13 shows the distribution of horizontal pressures on the wall, for different degrees of soil inhomogeneity (n) and wall flexibilities (d_w). The case of homogeneous soil as well as the parabolic case considered by Veletsos and Younan (V-Y), are also reported.

Evidently as soil inhomogeneity increases, the horizontal stresses on the wall decrease, the reduction being more important for rigid walls. As in the case of parabolic variation, a reduction of tensile stresses on the upper part is observed, especially for high values of n.

The reduction of stresses transferred from the soil to the wall, results in a reduction of internal forces, as shown in fig. 14 for base shear. The continuous lines show closed-form solutions for the homogenous case. As can be seen, there is an almost constant reduction of base shear with d_w, whereas a consistent reduction of base moment for rigid walls can be shown, as already seen in fig. 12.

In terms of effective height (fig. 15) these different reductions produce a reduction for rigid walls (around 0.5÷0.6 H, which is close to Seed and Whitman [1970] suggestion) whereas an increase is observed for flexible walls (clearly due to the reduction of tensile stresses on the upper part), moving towards the Rankine value ($H / 3$).

The simple assumption of soil inhomogeneity implies a reduction of internal forces in the wall, and therefore a more realistic simulation of the interaction between soil and retaining structure. Similar observations have been made by Psarropoulos *et al.* [2005].

As for the homogeneous case, dynamic results are omitted, as they are similar to the corresponding 'static' ones, since elastic behaviour has been assumed in this part of the analysis. In the following a more realistic non-linear elastic-plastic interaction simulation is attempted.

NON-LINEAR ELASTIC-PLASTIC PROBLEM

Since soil-wall interaction may involve significant levels of strain in the backfill, material non-linearity should be accounted for to realistically simulate the response (Callisto and Soccodato [2007]). Several studies have been carried out to assess, approximately, the main features of non-linear dynamic soil-wall interaction, but there is a lack of rigorous analyses. In the following, results of a series of parametric *fully non-linear* analyses will be presented, and a generalization of the results will be made, to provide a general framework for understanding complexities associated with the problem.

Description of the Model

The proposed model (fig. 16) is essentially a "box" in which a pair of vertical *flexible* cantilever walls, at a relative distance of 10 H, retains a horizontal layer of inhomogeneous soil. The material obeys an elastic-plastic Mohr-Coulomb criterion coupled with hysteretic damping, resulting from a strain-dependent modulus decay law.

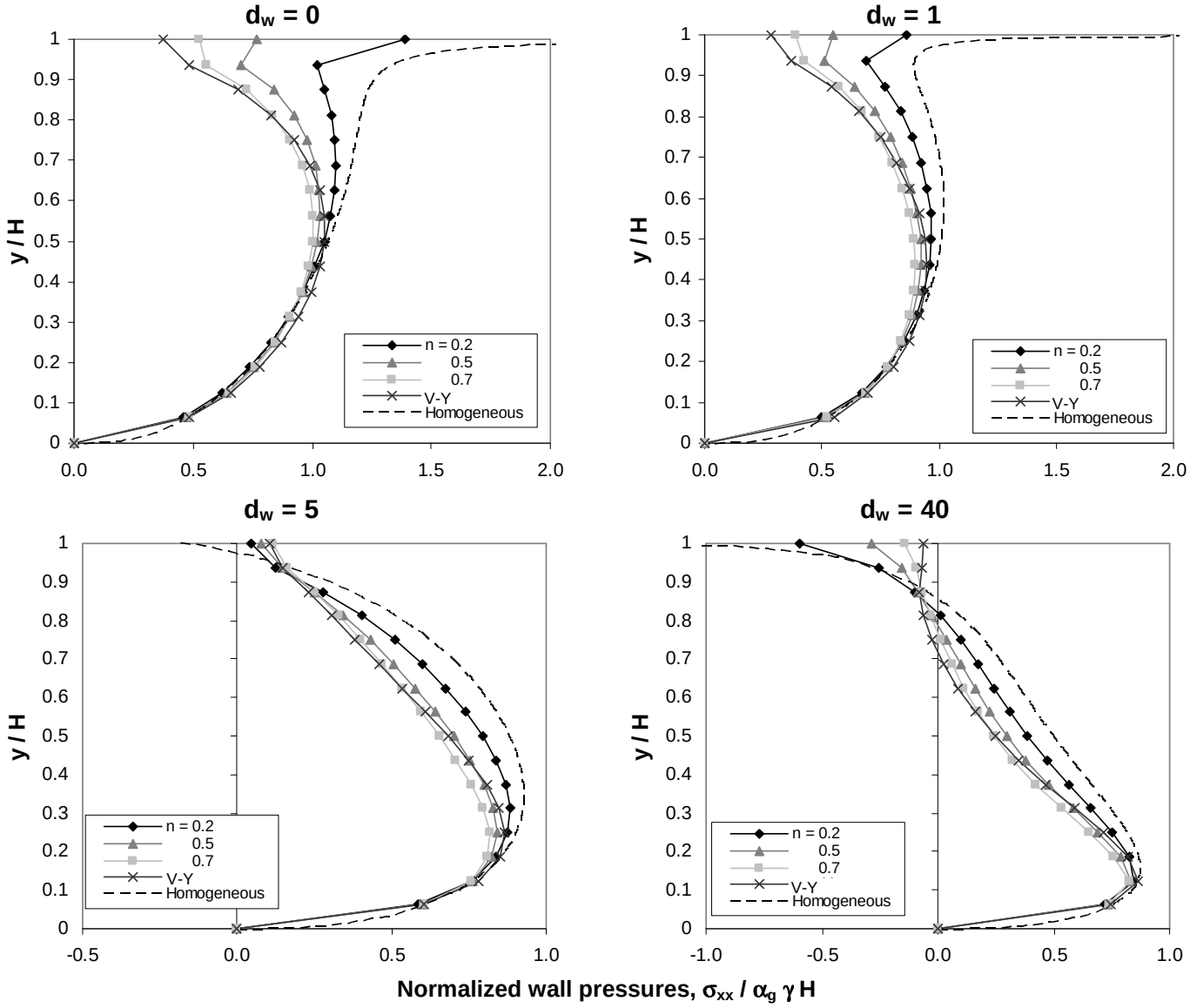

Fig. 13. Effects of soil inhomogeneity on wall pressures

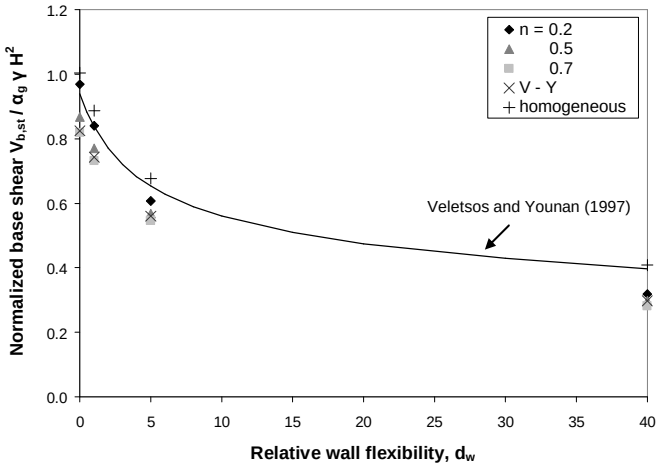

Fig. 14. Effects of soil inhomogeneity on base shear

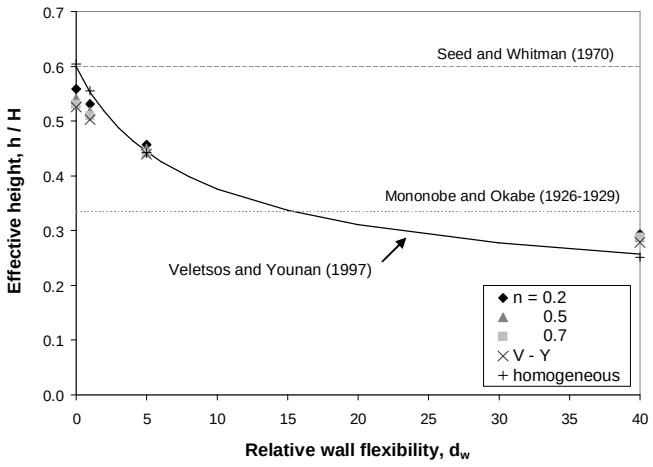

Fig. 15. Effects of soil inhomogeneity on effective height

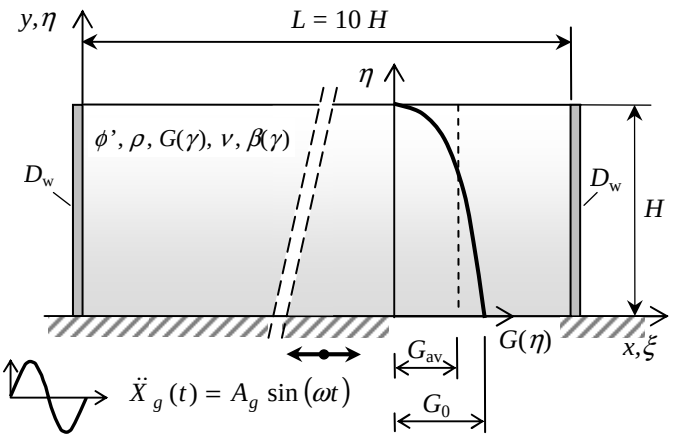

Fig. 16. Model proposed for non-linear analyses

The excitation ($\ddot{X}_g = a_g$) is a full cycle sinusoidal acceleration pulse with given amplitude and frequency applied at the bottom of the model.

The fundamental parameters of the problem are:

- shearing resistance angle: $\phi' = 35°$
- relative soil-wall flexibility: $d_w = 40$
- peak base acceleration: $A_g = (0.05 \div 0.35)$ g
- normalized excitation frequency: $\omega/\omega_1 = 1 \div 3$

The soil inhomogeneity is expressed via the exponential law (eqn. (12)) with n = 0.5, G_0 = 112.5 MPa ($V_{s,0}$ = 250 m/s, ρ = 1.8 Mg/m^3, ν = 1/3). The modulus decay law $G(\gamma)$ / G_{max} adopted for the soil (fig. 17), simulates the sand (upper range) law proposed by Seed and Idriss [1970]: the application of Masing rules automatically defines hysteretic damping of the soil $\beta(\gamma)$ (where γ is the shear strain). As it may be seen, FLAC largely overestimates the damping ratio after approximately γ = 0.3-0.4 %, but this was not the case in the performed analyses. A small amount of stiffness-proportional Rayleigh damping (0.5%) was added, since hysteretic damping provides almost no energy dissipation at very low cyclic strain levels, which may be unrealistic.

The wall height is H = 8 m and the wall is discretized by means of beam elements of unit longitudinal dimension and thickness $t_w \cong$ 0.73 m. The wall material is supposed to be concrete, with mass per unit of surface area μ_w = 2.5 Mg/m^2, Young modulus E_w = 28.5 GPa and Poisson's ratio ν_w = 0.2.

The fundamental frequency of the soil is only an estimate, since there is no closed form solution for an inhomogeneous soil with an exponential increase of shear modulus with depth. Trials were conducted to identify this frequency in elastic domain, although for non-linear soil these values are valid only for small strain level.

The computational steps were the following:

1. model the gravitational (initial) condition
2. model the pseudo-static condition ($\omega \approx 0$) and dynamic condition.

In the first step the gravity was applied to the model and the initial stresses were imposed to be the geostatic: $\sigma_{yy} = \rho\, g\, z$,

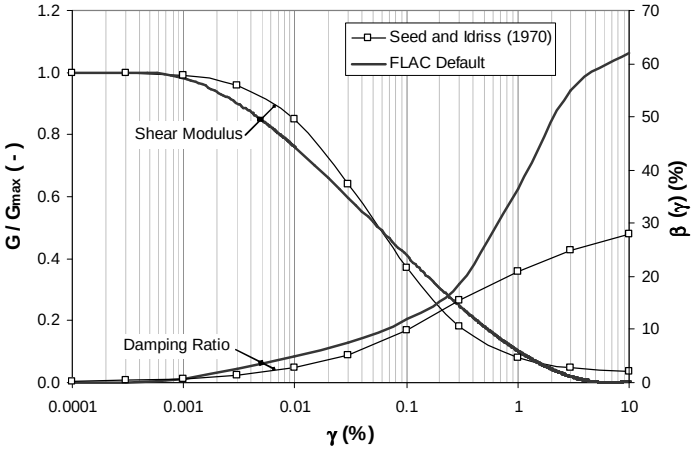

Fig. 17. Comparison between FLAC and Seed and Idriss [1970] modulus and damping ratio decay law for sands

$\sigma_{xx} = \sigma_{zz} = K_0 \cdot \sigma_{yy}$, where K_0 = 1 – sin ϕ' (Jaky, 1944) is the coefficient of earth pressure at rest.

Gravitational and Pseudo-Static Loading

Figure 18 shows the distribution of horizontal pressures behind the wall after gravitational loading, normalized to horizontal pressures at rest. Due to the large wall flexibility (d_w = 40), for a large part the soil behind the wall is close to plastic conditions, where K_a (active) conditions apply, whereas in the vicinity of the base (which is fixed against all movements) the pressures gradually move towards K_0 (at rest) conditions.

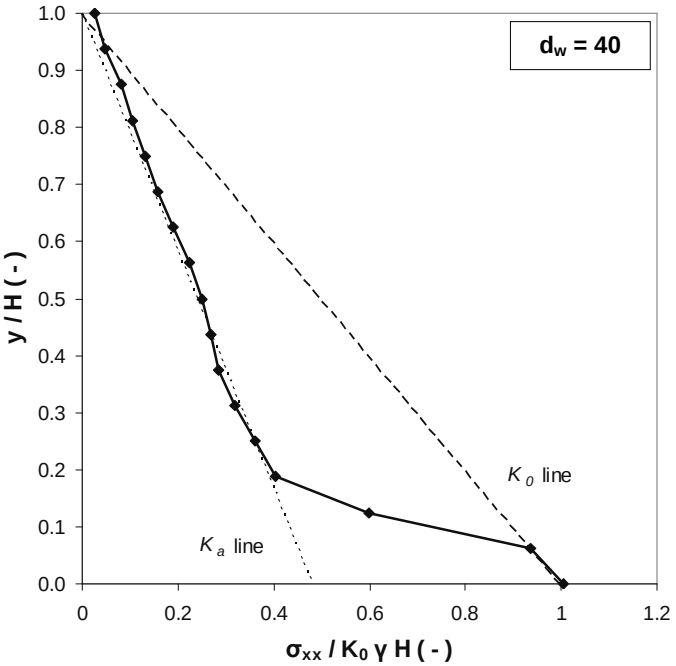

Fig. 18. Wall pressures after gravitational loading

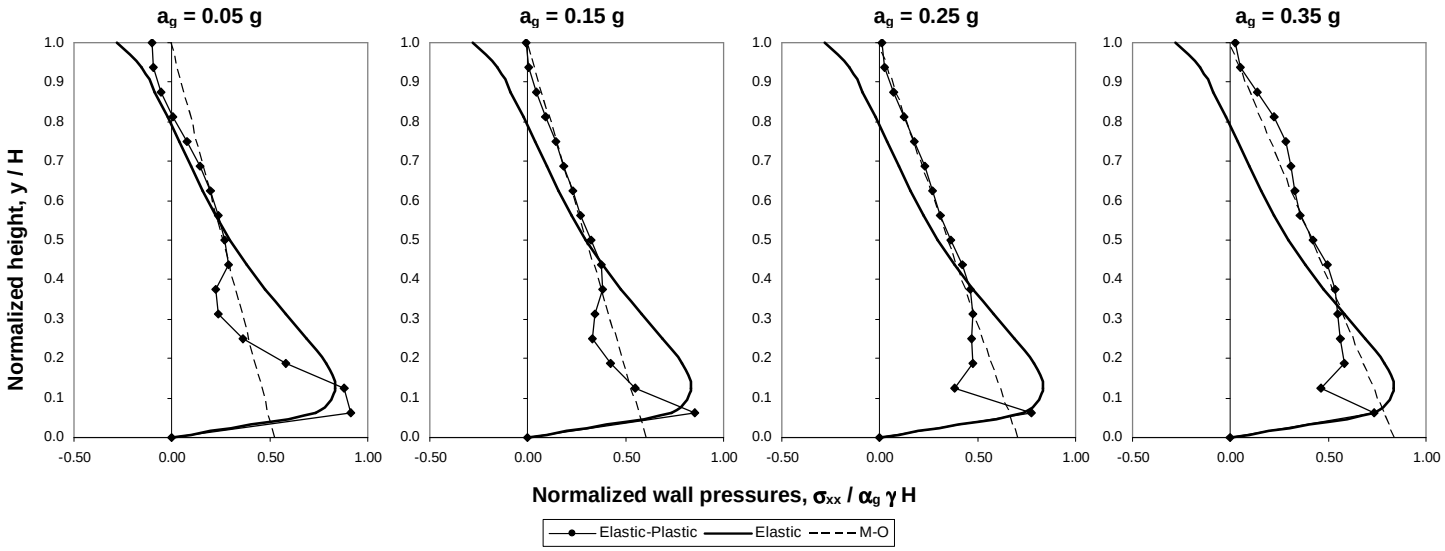

Fig. 19. Pseudo-static wall pressures for different acceleration levels

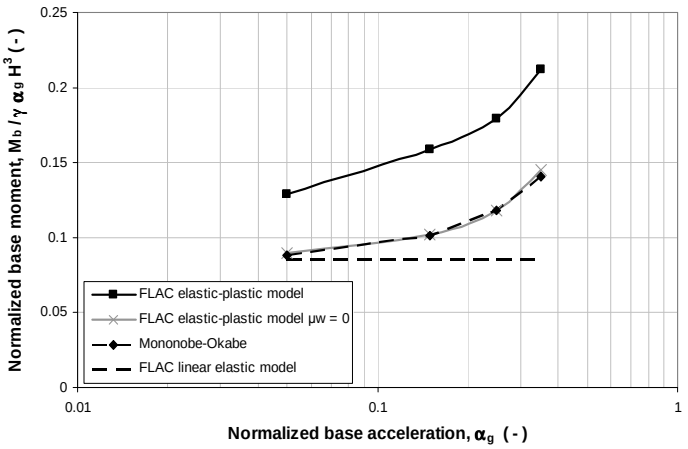

Fig. 20. Base moment due to pseudo-static loading

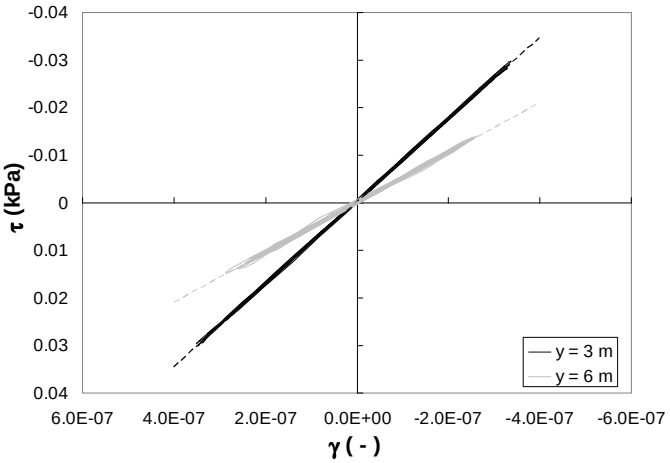

Fig. 21. Dynamic behaviour of soil at a_g = 0.0001 g

Following the gravitational phase the pseudo-static loading is applied. Figure 19 shows the distribution of pseudo-static pressures behind the wall (after subtracting gravitational pressures), as well as linear analyses results, shown in solid line. Very good agreement with M-O solution is found for all levels of ground acceleration taken into account. This is not surprising, since the model is now elastic-plastic and the loading is applied in a pseudo-static fashion.

It's interesting to notice that for low a_g values there is a reasonable agreement between elastic and elastic-plastic results, whereas with increasing a_g level this agreement is gradually lost (except for the lowest part of the wall where the fixity doesn't allow plastic deformation to occur). Therefore, a transition is observed from elastic behaviour, in which V-Y type methods seem to be applicable, to plastic behaviour in which M-O methods are thought to be more suitable under pseudo-static conditions. This transition becomes more or less important depending on the a_g imposed.

In terms of bending moments (fig. 20), a good comparison between pseudo-static and application of M-O formula is observed, taking into account the inertial effect due to wall mass, that obviously cannot be directly accounted for into M-O formula. Indeed, simulations with zero wall mass ($\mu_w = 0$) clearly point out this aspect. This was not so influent in elastic analyses because of the relatively small wall thickness t_w, contrary to the present problem, for which a realistic concrete wall with a specific thickness has been simulated.

Linear elastic results seem to provide a lower bound of elastic-plastic results (neglecting wall mass contribution). This is attributed to the improved simulation of soil-wall interaction phenomenon. Indeed, in elastic analyses complete bonding between soil and wall was assumed, leading to formation of tensile stresses near the top of wall. In the elastic-plastic case, Mohr-Coulomb criterion doesn't allow the tensile stresses to exceed the gravitational compressive stresses (see fig. 19, for a_g = 0.05 g, where tensile stresses do not exceed yet the gravitational compressive stresses, shown in fig. 18). As a result, an increase in stresses near the top of wall and in associated internal forces in the wall (shear and bending moment) is observed.

Therefore, the common thinking that considering elastic solutions is conservative does not apply for this case, mainly due to the large wall flexibility assumed.

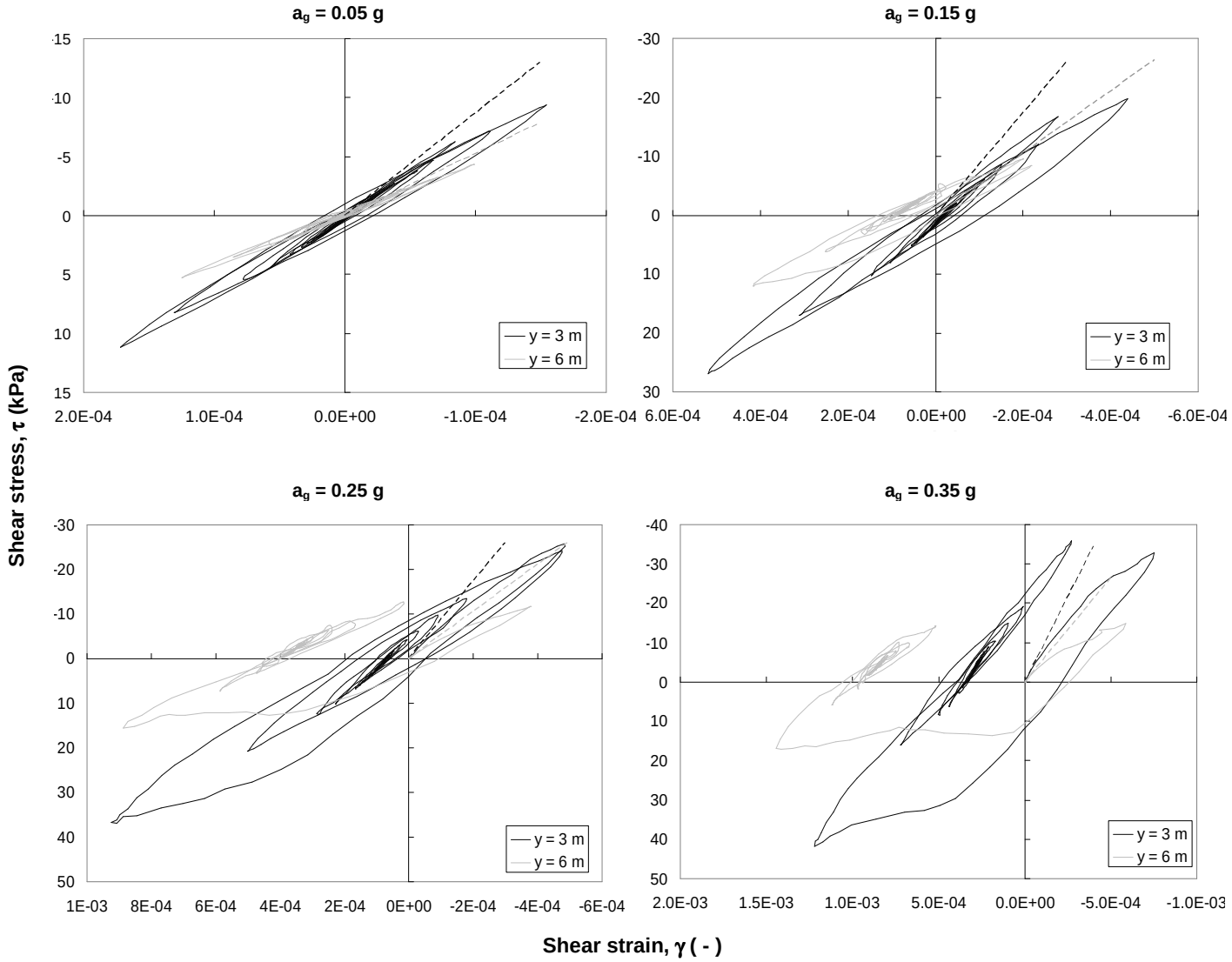

Fig. 22. Dynamic behaviour of soil for different acceleration levels

Dynamic Loading

Some preliminary analyses were conducted to check the response of the hysteretic model in FLAC. For this purpose, the dynamic behaviour of two soil elements located at $\xi = x / L = 0.5$ (*i.e.* on the centerline of the model), respectively at 3 and 6 m from the model base, was monitored. Single pulses with frequency equal to the fundamental, and acceleration levels from a_g = 0.05 to 0.35 g were applied, including a special case of a_g = 0.0001 g, representative of elastic conditions. The results are presented in the form of τ–γ curves in figures 21 and 22.

At a_g = 0.05 g (fig. 22), the behaviour is elastic, but some hysteretic damping is appearing, and the two soil elements show different damping since are subjected to different shear strain. When the acceleration is larger this damping is clearly increasing. When the base acceleration level becomes very high (*i.e.* above 0.15 g) plastic effects are observed, coherently with the hypothesis of elastic-plastic model: for 0.25 g and 0.35 g large plastic deformations are observed, and this plastic behaviour is also taking part in energy dissipation adding up extra damping to the hysteretic component.

Normalized pressures due to horizontal shaking decrease for increasing excitation, as shown in fig. 23, where corresponding elastic results are reported with a black solid line. This results in a reduction of internal forces acting on the structure, as shown in fig. 24. It's clearly visible that for the elastic-plastic model there is a decay in terms of normalized bending moment with acceleration level.

The elastic case is below the elastic-plastic case for the reasons discussed previously. Concerning the M-O formula, which cannot allow for any kind of dynamic effect, the results are well below elastic-plastic results.

Total (gravitational + dynamic) base moments $M_{b,tot}$ for all frequencies and acceleration levels are plotted in fig. 25. Horizontal line indicates the value of $M_{b,grav}$, that is the value of base moment for gravitational loading.

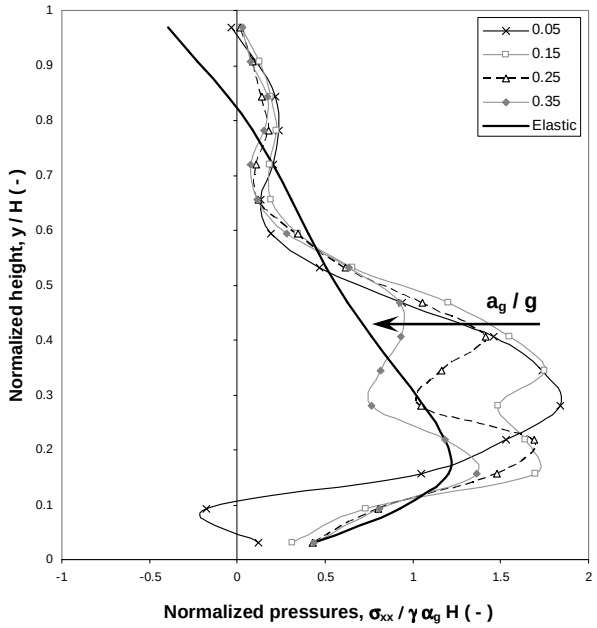

Fig. 23. Dynamic wall pressures at $\omega = \omega_1$

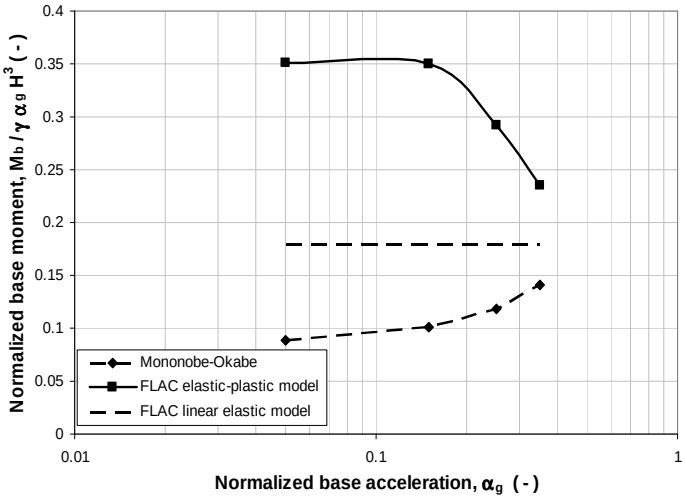

Fig. 24. Base moment due to dynamic loading ($\omega = \omega_1$)

It is clear that with increasing acceleration level, the base moment is increasing, but soil non-linearity effects are clearly visible: as acceleration level increases the "fundamental frequency" of the system is decreasing, due to *softening* of the soil material. Furthermore, for large acceleration levels (a_g / g = 0.35) the curve is not so regular, which can be attributed to larger plasticity effects in the soil. As frequency increases, base moment tends to move towards the gravitational value, since dynamic effects become less important.

It is instructive to introduce an *amplification factor* (fig. 26):

$$AF(M_b) = \frac{M_{b,tot} - M_{b,grav}}{M_{b,pst} - M_{b,grav}} = \frac{M_b}{M_{b,pst} - M_{b,grav}} \qquad (13)$$

where $M_{b,pst}$ is the *total* base moment for pseudo-static loading.

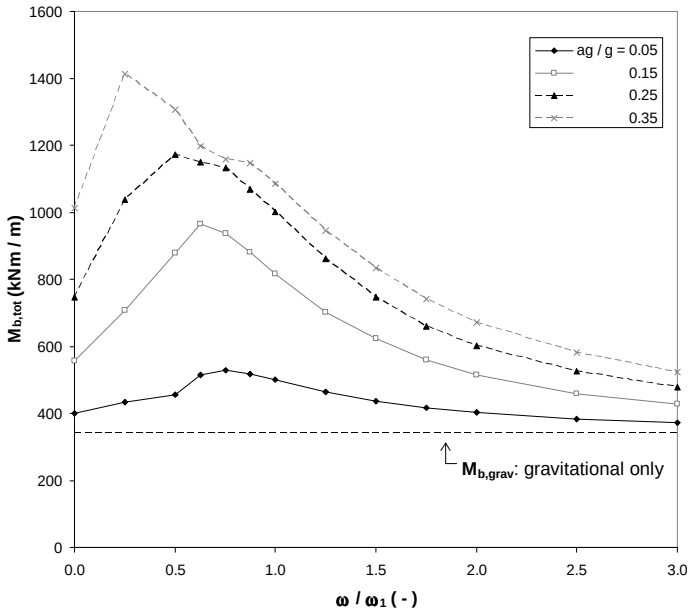

Fig. 25. Total base moment for different a_g / g and ω/ ω_1

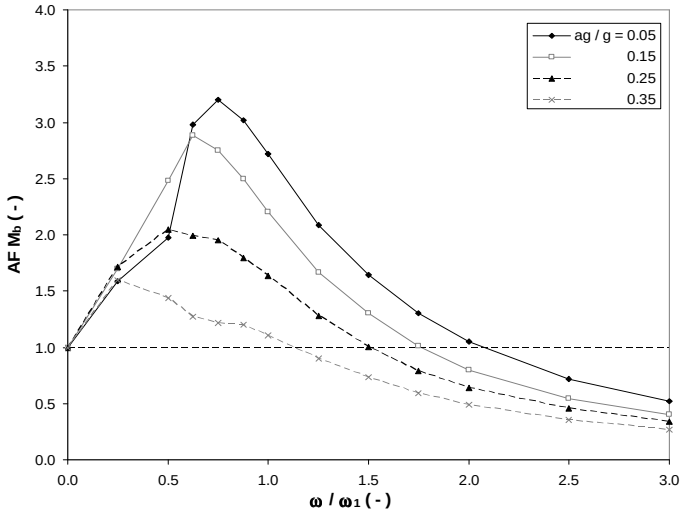

Fig. 26. Amplification factor for different a_g / g and ω/ ω_1

Analysing fig. 26 the following conclusions can be drawn:

- as acceleration level is increasing, $AF(M_b)$ is decreasing due to hysteretic damping and plasticity effects;
- as acceleration level is increasing, the "fundamental frequency" of the system is decreasing, due to soil softening;
- as excitation frequency is increasing there is deamplification (dynamic bending moment is lower than pseudo-static moment).

The effective height of the resultant dynamic force is located in the region of (0.3÷0.4) H as shown in fig. 27, hence in agreement with Rankine theory (1/3 H), and below EC8 part 5 [2004] suggestion (0.5 H) or Seed and Whitman [1970] suggestion (0.6 H).

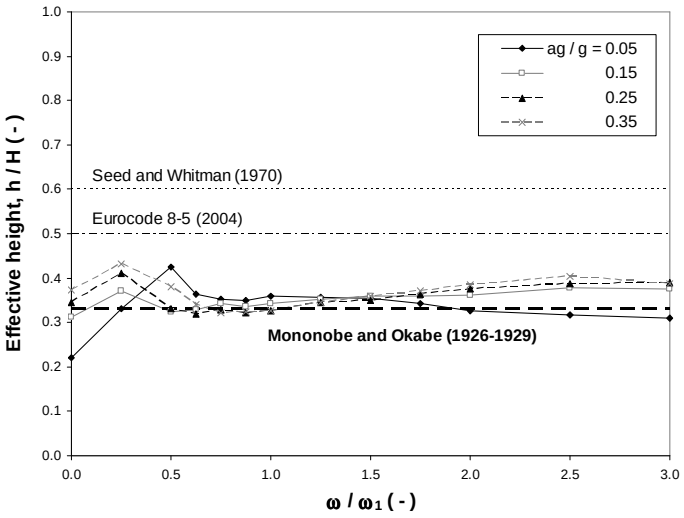

Fig. 27. Effective height for different a_g/g and ω/ω_1

FINAL REMARKS

Results of a series of numerical analyses with the finite-difference code FLAC presented in the present paper have demonstrated limits of applicability of both limit equilibrium and elastic methods in the computation of pressures behind rigid and flexible structures. The assumption of soil non-linearity has shown aspects that cannot be accounted for by means of these simplified approaches.

Improvements in elastic analyses have been achieved by means of the simple assumption of *soil inhomogeneity*, as already noted by Veletsos and Younan [1994, 1997], and Psarropoulos *et al.* [2005]: (1) a consistent reduction of internal forces acting on the structure is observed for rigid walls, and (2) tensile stresses near the top of wall for large wall flexibility or base compliance are reduced.

Elastic-plastic analyses for flexible walls have shown several important features: (1) *dynamic amplification* is important for excitation frequency between one and two times the fundamental of the soil layer, therefore the simple pseudo-static assumption of M-O method results in a underestimation of effects; (2) non-linearity implies *decrease of the resonant frequency* of the layer, as well as the important effect of *reduction of dynamic amplification effects* with increasing acceleration level, a beneficial effect which is impossible to take into account by means of M-O and V-Y methods.

In general, with the obtained informations non-linear dynamic soil-wall interaction effects for flexible walls are clarified, and a more comprehensive and innovative approach for analysis and design of earth retaining structures can be developed.

Current research is devoted to comparison of outcomes with available experimental findings, analysis of effects of real accelerograms, as well as the assumption of a plastic hinge at wall base, possibly leading to development of a *performance based approach* for the analysis of cantilever retaining walls.

REFERENCES

Arias, A., Sanchez-Sesma, F.J., Osvaldo-Shelley, E. [1981], "A simplified elastic model for seismic analysis of earth-retaining structures with limited displacements", *Proceedings of the International Conference on Recent Advances in Geotechnical Earthquake Engineering and Soil Dynamics*, University of Missouri, Rolla, MO, I, pp. 635-642.

Callisto, L., and Soccodato F.M. [2007], "Seismic analysis of an embedded retaining structure in coarse-grained soils", *4th International Conference on Earthquake Geotechnical Engineering*, June 25-28, Thessaloniki, Greece.

Comité Européen de Normalisation (CEN), [2004], EN 1998-5:2004 – "Eurocode 8: Design of structures for earthquake resistance - Part 5: Foundations, retaining structures and geotechnical aspects".

Mononobe, N. and Matsuo, H. [1929], "On the determination of earth pressures during earthquakes", *Proceedings of the World Engineering Congress*, vol. 9, pp. 179-187.

Okabe, S. [1926], "General theory of earth pressures", Journal of the Japan Society of Civil Engineering, Tokyo, vol. 12, n.1.

Psarropoulos, P.N., Klonaris, G., Gazetas, G. [2005], "Seismic earth pressures on rigid and flexible retaining structures", Soil Dynamics and Earthquake Engineering, Vol. 25, pp.795-809.

Richards, J. and Elms, D.G. [1979], "Seismic behaviour of gravity retaining walls", Journal of Geotechnical and Geoenvironmental Division, ASCE, 105(4), 449-464.

Seed, H.B., and Idriss, I. M. [1970], "Soil Moduli and Damping Factors for Dynamic Response Analysis," Earthquake Engineering Research Center, University of California, Berkeley, Report No. UCB/EERC-70/10, p. 48, Dec. 1970.

Seed, H.B., and Whitman, R.V. [1970], "Design of earth retaining structures for dynamic loads", *Proceedings of the special conference on lateral stresses in the ground and design of earth retaining structures*, pp. 103–147.

Veletsos, A.S. and Younan, A.H. [1994], "Dynamic modeling and response of soil-wall systems", Journal of Geotechnical and Geoenvironmental Engineering, ASCE, 120 (12), pp. 2155-2179.

Veletsos, A.S. and Younan, A.H. [1997], "Dynamic response of cantilever retaining walls", Journal of Geotechnical and Geoenvironmental Engineering, ASCE, 123 (2), pp. 161-172.

Wood, J. [1973], "Earthquake-induced soil pressures on structures", Report EERL 73-05, California Institute of Technology, Pasadena, California, 311 pp.